Stray light test station for measuring point source transmission and thermal background of visible and infrared sensors

Gary L. Peterson

Breault Research Organization, 6400 East Grant Road, Suite 350
Tucson, Arizona 85715

ABSTRACT

Breault Research Organization has designed and built a stray light test station. The station measures the point source transmission and background thermal irradiance of visible and infrared sensors. Two beam expanders, including a large 0.89 *meter* spherical mirror, expand and collimate light from laser sources at 0.658 and 10.6 μm. The large mirror is mounted on a gimbal to illuminate sensors at off-axis angles from 0° to 10°, and azimuths from 0° to 180°. Sensors with apertures as large as 0.3 *meters* can be tested with the existing facility. The large mirror is placed within a vacuum chamber so cryogenic infrared sensors can be tested in a vacuum environment. A dark cryogenic cold plate can be translated into the field of view of a sensor to measure its background thermal irradiance.

Keywords: stray light, test station, point source transmission

1. INTRODUCTION

Breault Research Organization has designed and built a stray light test station. The stray light test station is designed to measure stray light in sensors with apertures as large as 0.3 *meters*, and to perform these measurements at both visible and thermal infrared wavelengths. Two types of stray light measurements are possible: a point source transmission (PST) measurement to evaluate the response of sensors to illumination from external sources, and a thermal background measurement to evaluate stray light from internal thermal emission in infrared sensors. To characterize the directional dependence of point source transmission measurements, the test station illuminates sensors over off-axis angles from 0° to 10°, and azimuths from 0° to 180°.

2. DESCRIPTION AND CAPABILITIES

The stray light test station measures point source transmission (PST) by illuminating the entrance aperture of a sensor under test (hereafter referred to as *the sensor*) with laser light that is collimated by a large spherical mirror. Figures (1) and (2) illustrate the concept. The large mirror sits within a vacuum chamber, with the sensor mounted to a gate valve at one end. Lasers, beam control and conditioning optics, and a beam expander sit outside the chamber. The lasers and external optics produce a uniform flat-top beam with a diameter as large as 42 *mm*.

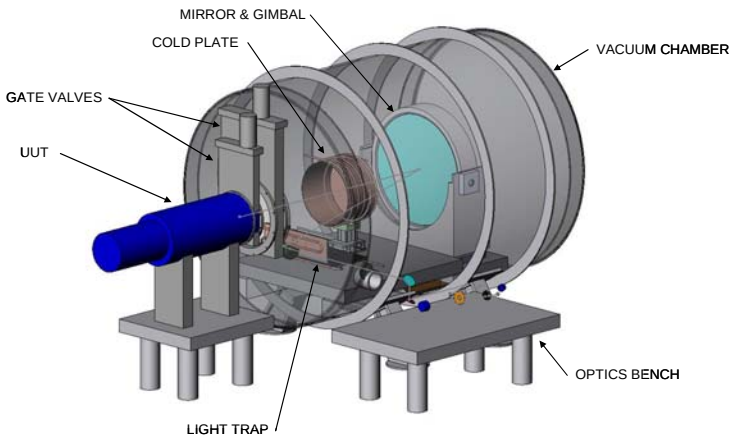

Figure (1): CAD model of the stray light test station.

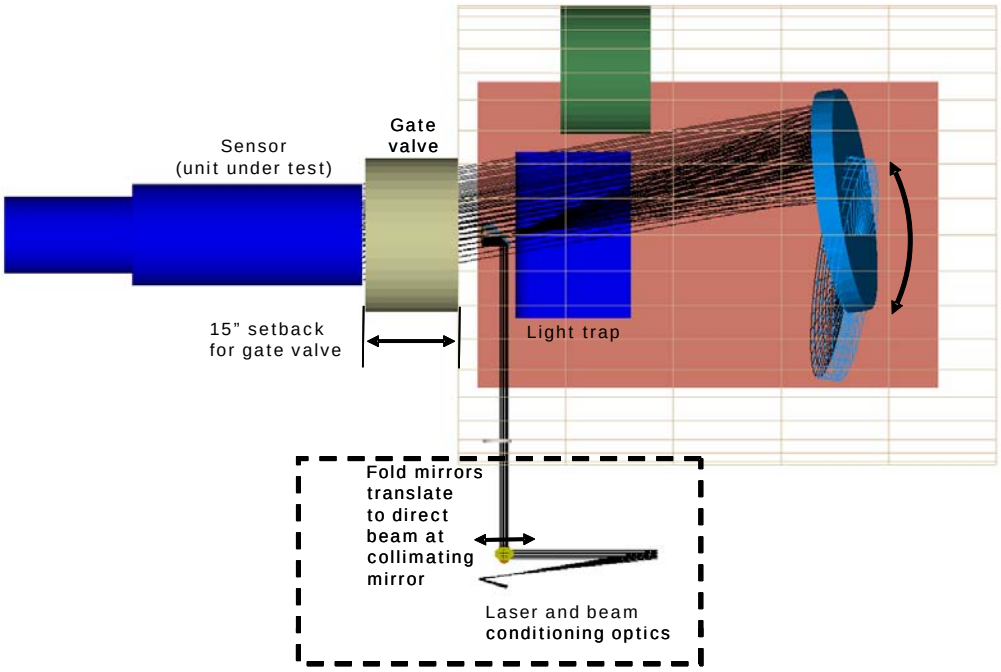

Figure (2): Illustration of laser light propagating through the stray light test station.

This beam is fed into the chamber through an anti-reflection-coated Cleartran™ window. A fold mirror in the chamber directs the beam to an off-axis parabola (OAP) which forms a point source for the large spherical mirror. The spherical mirror then collimates the light to illuminate the sensor.

Beam steering is done with two separate systems. The large collimating mirror is mounted on a two-axis gimbal. The gimbal rotates to vary the direction of the collimated beam. In addition, two periscope mirrors outside the chamber translate in two dimensions to steer the beam across the large mirror. This controls the location of the beam at the sensor entrance aperture. The four degrees of freedom afforded by the collimating mirror gimbal and periscope translation stage allow control over the two direction variables and two position variables of the beam at the sensor aperture. In addition, the collimating mirror gimbal is mounted on a horizontal translation stage. This reduces both the size of the mirror and the size of the vacuum chamber by expanding the range of illumination directions that can be accommodated with a relatively small mirror.

The sensor must stare at a dark scene during a stray light test. This prevents the low stray light signals from being swamped by radiation inside the sensor's field of view. At thermal infrared wavelengths the scene must also be cold. A light trap mounted to the floor of the chamber supplies this cold dark scene. It is an L-shaped plate that intercepts the sensor field of view over the full range of available test directions. A small hole in the light trap passes radiation from the OAP to the large collimating mirror. The hole is placed near focus to minimize its size. The light trap is coated with Vel-Black™, a black applique with a diffuse reflectance that is less than 1% at both visible and infrared wavelengths. Liquid nitrogen is pumped through the pipes within the light trap to cool it to cryogenic temperatures.

The sensor sees the light trap reflected in the collimating mirror. This mirror rotates and translates, so the light trap is sized and shaped to intercept the sensor's field of view for all illumination directions. Rays traced from within the sensor's field of view are shown in Figure (3). They illustrate how the field of view scans across the light trap as the mirror is moved. The L-shape of the light trap minimizes its size. It also prevents grazing incidence scatter paths from the light trap surfaces to the sensor.

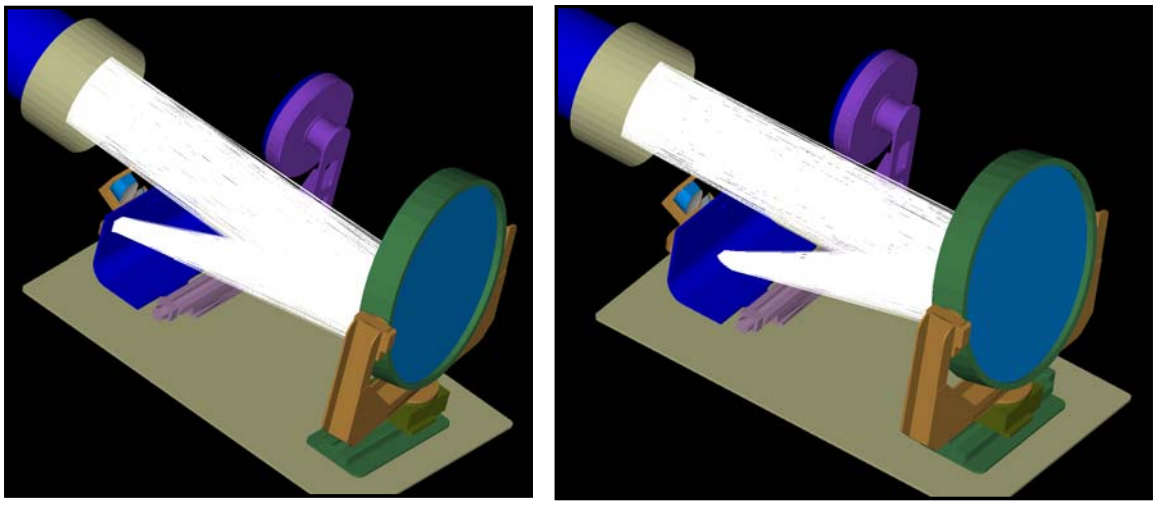

Figure (3): Ray traces from the sensor show how the sensor's field of view scans across the light trap as the collimating mirror shifts and rotates.

Because the sensor stares at illuminated areas of the primary mirror, a low scatter mirror is fundamental to the performance of the test station. The existing mirror has a root-mean-square (rms) roughness in the neighborhood of 10 *Angstroms*. CO_2 snow equipment is used to clean the mirror. The chamber sits within a clean tent to minimize contamination of the mirror when the chamber is open. However, the vacuum environment of the chamber is the principal means of maintaining mirror cleanliness.

The station optics and light trap are designed to accommodate sensor fields of view as large as 2°×2° over off-axis angles as large as 10° and apertures as large as 0.4 *meters*. Fields of view as large as 5°×5° can be accommodated if the sensor aperture is less than 0.25 *meters*.

For cost considerations, the station is currently equipped with a small gate valve that limits the aperture to 0.3 *meters*. The test station optics can accommodate sensor apertures as large as 0.4 *meters* if a larger gate valve is used. Sensors can be illuminated over a range of directions that subtend off-axis angles as high as 10°, and azimuths from 0° to 180°.

The test station currently has a visible and an infrared laser source. The visible source is a 60 *mW* BlueSky™ fiber coupled laser emitting at a wavelength of 0.658 μm. The infrared source is a 12 *Watt* Lasy 12 CO_2 laser from Access Laser Company.

Internal thermal background measurements are done by moving a *cold plate* in front of the sensor. This is illustrated in Figure (4). The cold plate is manufactured by ATK Mission Research. The face of the cold plate has a series of concentric V-grooves coated with Aeroglaze Z302, a specular black paint, to absorb incident radiation. The cold plate moves to the side of the chamber during the PST test.

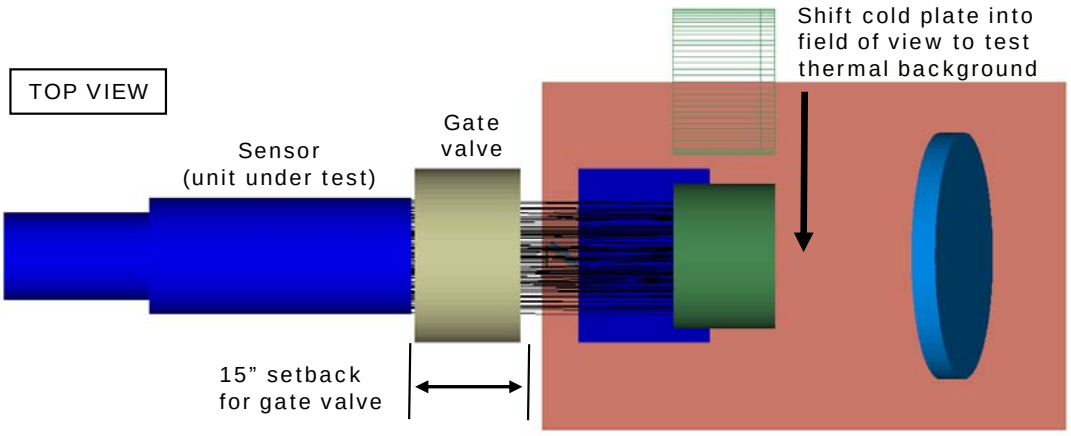

Figure (4): Illustration of how a cold plate moves into the field of view of the sensor during a thermal background test.

III. MEASURED PERFORMANCE AT VISIBLE WAVELENGTHS

Functional tests have verified that the test station performs properly at visible wavelengths. Beam size was verified by inspection. Collimation and beam direction were verified with a Hartmann test. Power measurements verified beam irradiance uniformity.

A diffuse Mylar® screen was placed over the chamber exit port prior to installation of the gate valve. Figure (5) is a photograph of the screen illuminated by the collimated visible beam. The exit port on the chamber is 20 *inches* in diameter. The beam diameter is somewhat greater than 16 *inches*. The beam is not centered on the aperture in this picture because the periscope mirrors outside the chamber were not well positioned at that time. Large scale variation in the apparent brightness across the beam is not real. It is caused by changes in scatter angle from the Mylar film to the camera.

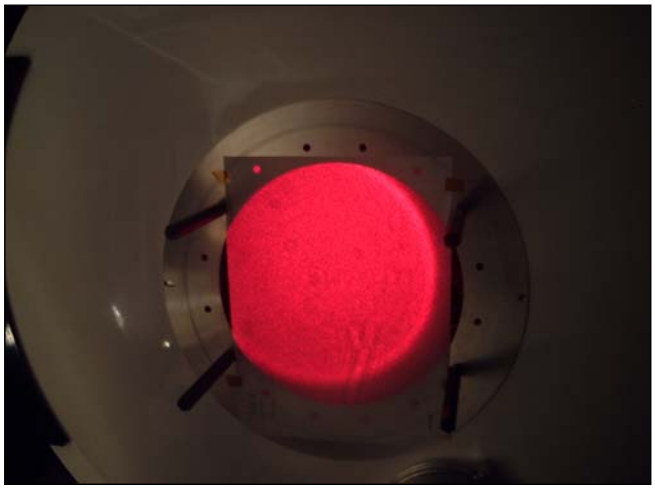

Figure (5): Photograph of the beam incident on a Mylar sheet at the chamber exit.

A *Hartmann test* was used to measure beam direction and collimation. It works by passing the beam through a plate with an array of holes (the Hartmann screen) and then observing the lateral displacement of the spots on a diffuse screen placed downstream of the plate. Our Hartmann screen consists of a circular metal plate with 0.156 *inch* diameter holes spaced at 1 *inch* intervals. The size of the plate exceeds 0.43 *meters*, which is sufficient to measure a 0.4 *meter* beam with ample margin for mounting. A diffusing screen, actually just a large sheet of white paper with printed circle and crosshair patterns, is placed 14.18 *inches* downstream of the Hartmann screen to view the transmitted spots. A 10° beam angle displaces the transmitted spots by 2.500 *inches*.

Verification of beam direction and collimation were done by visual inspection of the illuminated spots on the diffusing screen. To help with this inspection an array of crosshairs and circles were printed on the screen. The array has a pitch of 0.5 *inches*. When the beam direction is changed in increments of 2°, the array of spots shifts to adjacent crosshairs, so the screen does not have to be moved to realign the spots with the crosshairs. The diameter of circles

around each crosshair in the array was set so that if the array of illuminated spots lie entirely within their circles, then the pointing and wavefront errors meet their specifications.

Hartmann tests were performed at beam directions (θ,φ) of (0°,0°), (10°,0°), (10°,45°), (10°,90°), (10°,135°), and (10°,170°). In all cases, all or the vast majority of the spots were inside the outer circle. A small number of spots had approximately 5% of their energy outside the outer circle of the test pattern. This small discrepancy was judged to be acceptable, as there was some margin in the error budget absorb the discrepancy. Figure (6) shows a photograph of the Hartmann spots on the test pattern. Close inspection show illuminated spots centered on every other test pattern within the array.

The Hartmann screen was also used to measure the irradiance and its uniformity. A Gamma Scientific™ radiometer with a 1 cm^2 detector was placed behind the holes in the Hartmann screen to measure the power passing through them. By rastering the detector across a row or column of holes a measured cross-section of the irradiance with samples at 1-inch intervals was generated. Figure (7) shows detector power (arbitrary units) at horizontal and vertical cross-sections through the middle of the beam. The standard deviation taken over all of the measured points in Figure (7) that are inside a 0.33 *meter* diameter is ±12%.

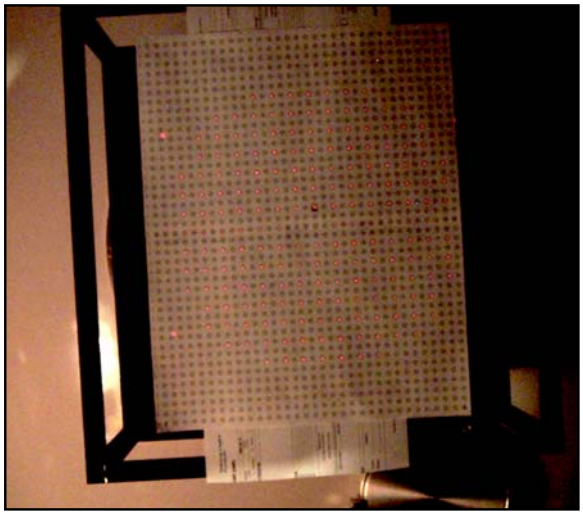

Figure (6): Photograph of Hartmann test that shows an array of illuminated circles centered on the test patterns.

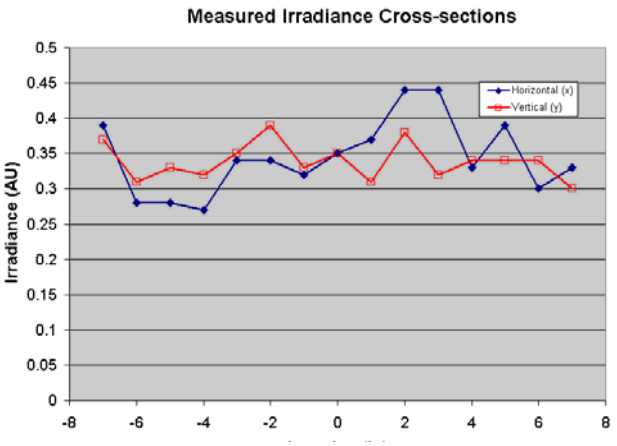

Figure (7): Beam irradiance as a function location on a vertical and horizontal cross section.

IV. STRAY LIGHT ANALYSIS OF THE TEST STATION

An operational stray light requirement for the stray light test station is that it measure the stray light irradiance (power/unit-area), or point source transmission, of a sensor without substantial corruption of the measurement by stray light from the station itself. Point source transmission (PST) is defined as the ratio of stray light irradiance on a detector to source irradiance at the entrance to a sensor. PSTs of sensors varies widely, but at 10° off-axis a well baffled system with clean well-polished mirrors may be expected to have a PST between 10^{-5} and 10^{-4} at visible wavelengths, and perhaps a factor of 5 lower at thermal infrared wavelengths. At smaller illumination angles the PST of a sensor will be larger. Well-baffled systems illuminated at small off-axis angles (less than or around 10° to 20°) are typically dominated by scatter from their mirrors or lenses. For these systems the PST varies approximately as $\sin^{s}\theta$, where θ is the off-axis angle and the slope s is typically around -2. From this we derive an angle-dependent objective for the sensor PST that must be measured:

$$PST_{sensor} \geq 1\times10^{-5}\left(\frac{\sin\theta}{\sin 10^{\circ}}\right)^{-2} \quad \text{at visible wavelengths,} \tag{1}$$

$$PST_{sensor} \geq 2\times10^{-6}\left(\frac{\sin\theta}{\sin 10^{\circ}}\right)^{-2} \quad \text{at infrared wavelengths.} \tag{2}$$

To characterize the stray light performance of the chamber we define an *effective PST* as

$$PST_{eff} = \frac{E_s}{E_o} \tag{3}$$

where E_s is the stray light irradiance produced by stray light within the test station at the focal plane of a sensor, and E_o is the irradiance that illuminates the entrance aperture of the sensor. To measure PSTs as low as those given by Equations (1) and (2), we want the effective PST from the chamber to be substantially less than the measured PST of the sensor.

Stray light analysis is simplified by restricting attention to objects that are seen directly by the sensor's detector. These are the so-called *critical objects*. In fact, the sensor sees only two objects within the chamber: the collimating mirror and the light trap. These two critical objects will supply practically all of the stray light to the sensor.

The collimating mirror is directly illuminated by the test beam. Depending on the size of the sensor aperture, much of the illuminated area is seen by the sensor. Figure (8) shows the overlap between the beam and the field of view of the sensor on the collimating mirror for three different illumination directions. These footprints are for a 0.4-meter diameter aperture (worst case). The overlap is almost complete at 2°, but is rather small at 10°. Some of the light in the overlap region will scatter directly from the collimating mirror into the field of view of the sensor. This is why the collimating mirror must be both smooth and clean. We must keep the amount of scattered light from the collimating mirror below the stray light level of the sensor itself.

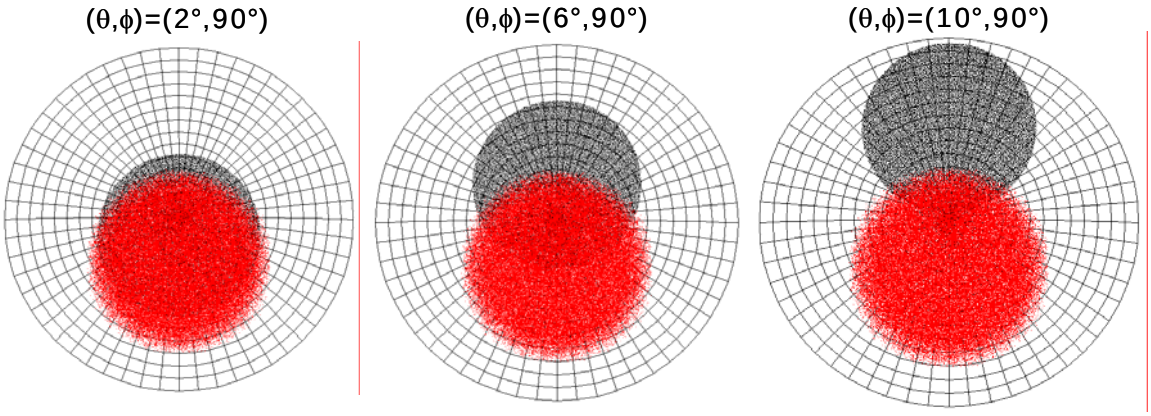

Figure (8): Footprints of the beam (dark spots) and 2°×2° sensor field of view (light/red spots) on the collimating mirror at three beam directions.

The second source of stray light is scatter from the light trap. The light trap is not directly illuminated by the beam, but some of the light that illuminates the sensor will scatter or reflect to the light trap, either directly or after reflection from the collimating mirror. In addition, light that overfills the sensor can scatter from surrounding gate valve surfaces to the light trap. Finally, scattered or reflected light from the sensor or gate valve that illuminates the shiny metallic chamber walls may find its way to the light trap after one or more bounces within the chamber.

Stray light calculations for the SLTS were done with BRO's Advanced Systems Analysis Program (ASAP™). Monte Carlo ray traces were done through a computer model of the chamber and its optical components. The model included both optical and mechanical components, and optical properties such as reflectance, transmittance, and scatter. The magnitude and distribution of scatter were described in terms of a bi-directional reflectance distribution function (BRDF). Mathematical models of the BRDF for the mirrors and mechanical surfaces were used during the ray trace to scale the power of rays as they are scattered within the model.

Elevation	Azimuth	Light trap PST	Mirror PST	Total PST
2	0	5.6E-07	6.87E-05	6.9E-05
2	45	5.6E-07	7.15E-05	7.2E-05
2	90	4.2E-07	7.25E-05	7.3E-05
2	135	4.9E-07	7.09E-05	7.1E-05
2	180	6.3E-07	6.93E-05	7.0E-05
6	0	4.9E-07	4.31E-06	4.8E-06
6	45	2.8E-07	4.55E-06	4.8E-06
6	90	2.1E-07	4.78E-06	5.0E-06
6	135	2.8E-07	4.39E-06	4.7E-06
6	180	5.6E-07	4.30E-06	4.9E-06
10	0	3.5E-07	2.65E-07	6.1E-07
10	45	1.4E-07	3.09E-07	4.5E-07
10	90	1.4E-07	3.28E-07	4.7E-07
10	135	1.4E-07	2.81E-07	4.2E-07
10	180	3.5E-07	2.78E-07	6.3E-07

Table (1): Effective PST at the center of a sensor detector, and contributions from the light trap and collimating mirror, as a function illumination direction at a wavelength of 0.633 μm.

Stray light calculations for the light trap require a model for the sensor, because much of the light that illuminates the light trap comes from reflection and scatter from the sensor. A simple Cassegrain-like telescope was assumed. It had a parabolic primary mirror with a diameter of 14 *inches*, a secondary mirror with a flat black coating on its back surface (which faces into the chamber), and a 16-inch cylindrical baffle that surrounded the primary and secondary mirrors. This model was used only to reflect and scatter light back into the chamber. Neither its imaging properties nor its internal stray light characteristics were used.

Table (1) and Figure (9) summarize the results of stray light calculations performed for the sensor at a wavelength of 0.658 μm. These calculations assumed a 0.4-meter diameter aperture on the sensor, an optical transmission (including central obscuration) of 70%, and a sensor numerical aperture of 0.1.

Inspection of Table (1) shows that at visible wavelengths scatter from the collimating mirror is the largest source of stray light for most illumination directions. This is particularly true at the smaller elevation angles. At and around an elevation angle of 10° the light trap and collimating mirror make similar contributions.

The data in Table (1) is plotted in Figure (9), along with the minimum sensor PST from Equation (1). The blue squares in Figure (9) are the effective PST at a wavelength of 0.658 μm. There are fifteen points altogether (some overlapping) representing calculations at three elevation angles (2°, 6°, and 10°) and five azimuths (0°, 45°, 90°, 135°, and 180°). The minimum sensor PST requirement is shown by the solid red curve. Inspection shows that the effective PST of the test station is lower than the sensor PST at all illumination directions.

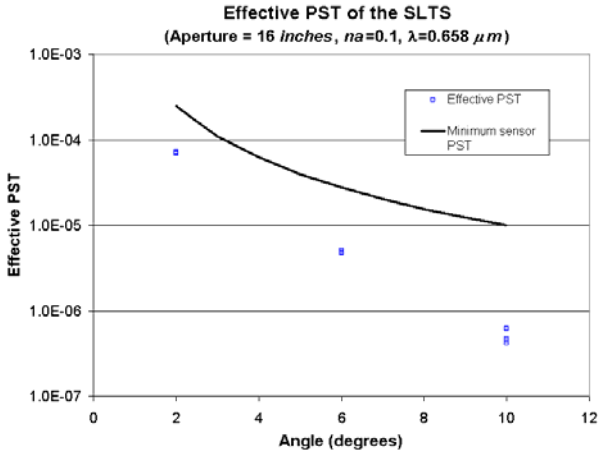

Figure (9) Effective PST (blue squares) and minimum sensor PST as a function of off-axis illumination angle (elevation) at a wavelength of 0.658 μm.

Table (2) and Figure (10) summarize the results of stray light calculations at a wavelength of 10.6 μm. Scatter from the mirror still dominates at small elevation angles (2°), but stray light from the light trap and mirror are comparable at intermediate elevations (6°), and the light trap dominates at large elevations (10°). The blue squares in Figure (10) are the effective PST at a wavelength of 10.6 μm. There are again fifteen points altogether (some overlapping) representing calculation at three elevation angles (2°, 6°, and 10°) and five azimuths (0°, 45°, 90°, 135°, and 180°). The PST objective, from Equation (2), is again shown by the solid red curve.

Elevation	Azimuth	Light trap PST	Mirror PST	Total PST
2	0	5.6E-07	2.75E-05	2.8E-05
2	45	5.6E-07	2.88E-05	2.9E-05
2	90	4.2E-07	2.94E-05	3.0E-05
2	135	4.9E-07	2.86E-05	2.9E-05
2	180	6.3E-07	2.78E-05	2.8E-05
6	0	4.9E-07	9.00E-07	1.4E-06
6	45	2.8E-07	9.63E-07	1.2E-06
6	90	2.1E-07	1.02E-06	1.2E-06
6	135	2.8E-07	9.30E-07	1.2E-06
6	180	5.6E-07	8.99E-07	1.5E-06
10	0	3.5E-07	4.01E-08	3.9E-07
10	45	1.4E-07	4.73E-08	1.9E-07
10	90	1.4E-07	5.07E-08	1.9E-07
10	135	1.4E-07	4.28E-08	1.8E-07
10	180	3.5E-07	4.21E-08	3.9E-07

Table (2): Effective PST at the center of a sensor detector, and contributions from the light trap and collimating mirror, as a function illumination direction at a wavelength of 10.6 μm.

A path table for stray light from the light trap at (θ,φ)=(10°,90°) is given in Table (3). The table expresses a stray light path as a sequence of scatters or reflections (*reflect*) with arrows indicating propagation from one object to another. Propagation through the normal sequence of objects is suppressed. For example, in Table (3) light in the first path starts at the source (S), goes through all of the optics in the beam train (not shown), and illuminates the sensor primary mirror. Light is then reflected from the sensor primary to the chamber walls, scatters again to the chamber walls, scatters to the collimating mirror and is reflected from the collimating mirror down onto the light trap. Finally, light is scattered from the light trap through the large collimating mirror to the sensor detector (*Det*). The column labeled *Perc* is the percent of the total stray light from the light trap that is contributed by this path. A running sum of the percent contributions from each path is shown in the last column.

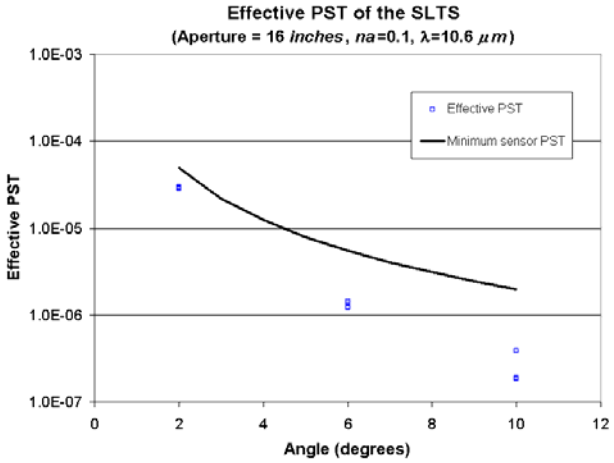

Figure (10): Effective PST (blue squares) and minimum sensor PST as a function of off-axis illumination angle (elevation) at a wavelength of 10.6 μm.

#	Path	Perc	Cum
1	S → Primary (reflect) → Chamber → Chamber → Mirror (reflect) → Light trap → Det	42	42
2	S → Primary (reflect) → Gate valve tube → Chamber → Light trap → Det	13	55
3	S → Gate valve end → Mirror (reflect) → Light trap → Det	13	68
4	S → Primary (reflect) → Gate valve tube → Mirror (reflect) → Light trap → Det	9	77
5	S → Gate valve tube → Primary (reflect) → Mirror (reflect) → Light trap → Det	4	81
6	S → Primary (reflect) → Mirror mount → Light trap→ Det	4	85
7	S → Primary (reflect) → Mirror mount → Chamber wall → Light trap → Det	4	89
8	S → Primary (reflect) → Mirror mount → Light trap → Det	2	91

Table (3): Path table for stray light from the light trap at (θ,φ)=(10°,90°).

Inspection of the table shows significant contributions from a number of paths. Scatter from the chamber walls is the largest stray light path, and plays a role in several other paths as well. Nevertheless, the overall magnitude of stray light from the light trap, as given in Tables (1) and (2), is acceptable, so the bright metallic walls of the chamber do not prevent the test station from meeting its stray light requirement.

V. SUMMARY

Breault Research Organization has designed and built a stray light test station to measure point source transmission at visible and thermal infrared wavelengths, and thermal background in infrared sensors. The performance has been tested at visible wavelengths. Source construction and testing at thermal infrared wavelengths is nearing completion. A stray light analysis shows that the test station can measure point source transmission at off-axis angles of 10° as low as 1×10^{-5} at visible wavelengths, and 2×10^{-6} at thermal infrared wavelengths.